Analytica Chimica Acta 1175 (2021) 338745

Contents lists available at ScienceDirect

Analytica Chimica Acta

journal homepage: www.elsevier.com/locate/aca

Fluorescence "turn-off/turn-on" biosensing of metal ions by gold nanoclusters, folic acid and reduced graphene oxide

Xin Yi Wong [a], Daniel Quesada-González [b], Sivakumar Manickam [a, c, d], Kasturi Muthoosamy [c, *]

[a] Department of Chemical and Environmental Engineering, Faculty of Science and Engineering, University of Nottingham Malaysia, 43500, Semenyih, Selangor, Malaysia
[b] Paperdrop Diagnostics, Av. de Can Domènech S/n, Eureka Building, Campus UAB, 08193, Bellaterra, Barcelona, Spain
[c] Nanotechnology Research Group, Centre of Nanotechnology and Advanced Materials, University of Nottingham Malaysia, 43500, Semenyih, Selangor, Malaysia
[d] Petroleum and Chemical Engineering, Faculty of Engineering, Universiti Teknologi Brunei, Bandar Seri Begawan, BE1410, Brunei Darussalam

HIGHLIGHTS

- A protein-gold nanoclusters (NCs)-based metal ions nanobiosensor is developed.
- The metal ions nanobiosensor is centered on fluorescence "turn-off/turn-on" strategy.
- The nanobiosensor is comprised of folic acid, reduced graphene oxide and NCs.

GRAPHICAL ABSTRACT

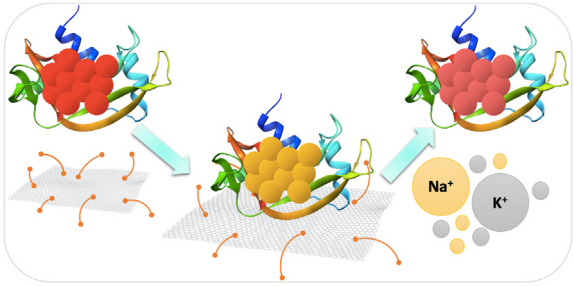

ARTICLE INFO

Article history:
Received 17 March 2021
Received in revised form
30 May 2021
Accepted 5 June 2021
Available online 10 June 2021

Keywords:
Gold nanoclusters
RNase A protein
Reduced graphene oxide
Metal ions
Nanobiosensor
Fluorescence

ABSTRACT

Metal ions homeostasis plays an important role in biological processes. The ability to detect the concentration of metal ions in biological fluids is often challenged by the obvious interference or competitive binding nature of other alkaline metals ions. Common analytical techniques employed for metal ions detection are electrochemical, fluorescence and colorimetric methods. However, most reported metal ions sensors are complicated, time-consuming and involve costly procedures with limited effectiveness. Herein, a nanobiosensor for detecting sodium and potassium ions using folic acid-functionalised reduced graphene oxide-modified RNase A gold nanoclusters (FA-rGO-RNase A/AuNCs) based on fluorescence "turn-off/turn-on" is presented. Firstly, a facile and optimised protocol for the fabrication of RNase A/AuNCs is developed. The activity of RNase A protein after the formation of RNase A/AuNCs is studied. RNase A/AuNCs is then loaded onto FA-rGO, in which FA-rGO is used as a potential carrier and fluorescence quencher for RNase A/AuNCs. Finally, a fluorescence "turn-on" sensing strategy is developed using the as-synthesised FA-rGO-RNase A/AuNCs to detect sodium and potassium ions. The developed nanobiosensor revealed an excellent sensing performance and meets the sensitivity required to detect both sodium and potassium ions. To the best of our knowledge, this is the first work done on determining the RNase A protein activity in RNase A/AuNCs and exploring the potential application of RNase A/AuNCs

* Corresponding author. Block B, University of Nottingham Malaysia, Jalan Broga, 43500, Semenyih, Selangor, Malaysia.
E-mail address: Kasturi.Muthoosamy@nottingham.edu.my (K. Muthoosamy).

https://doi.org/10.1016/j.aca.2021.338745

as a metal ion sensor. This work serves as a proof-of-concept for combining the potential of drug delivery, active targeting and therapy on cancer cells, as well as biosensing of metal ions into a single platform.

1. Introduction

Many studies have found a correlation between metal ions and biological processes such as kidney function, muscle contraction, blood pressure regulation, nerve transmission, autophagy, apoptosis, *etc.* [1–3]. Metal ions detection in a biological fluid is challenging due to the obvious interference or competitive binding nature of other alkaline metals ions [4]. This restricts the sensor with limited selectivity against other alkali ions, especially in aqueous solutions [2]. Common analytical techniques employed for metal ions detection are electrochemical, fluorescence and colorimetric methods. Electrochemical methods, such as the potassium ion (K^+) electrode, give reliable data with low detection limits (as low as 2.3 nM) [5]. However, it is limited to non-invasive study in biological systems due to the complicated nature of real sample matrices. The electrochemical method is only suitable for large volumes (higher than a few to tens of pico-litres) with large cell numbers. In contrast, the fluorescence method stands out as it is convenient, non-invasive, disposable, can be miniaturised and allows real-time *in situ* response [5,6]. "Turn-off" fluorescence assay is usually less sensitive than "turn-on" assay [7].

Oligonucleotide aptamers [2,8], single-layer graphene [3], valinomycin [9], 18-Crown-6 ether [10], *etc.*, are some of the sensing elements used for selective and sensitive detection of K^+. Triazacryptand (TAC) is typically used in designing biosensor for K^+, owing to its ability as a K^+ binding ligand and selective response for K^+ over competing for sodium ion (Na^+) [1,11]. Recently, a fluorescent K^+ sensor composed of TAC and rhodamine analog (as the fluorophore) has been used for monitoring the regulation of K^+ in mitochondria during apoptosis [1]. The as-synthesised sensor exhibited the largest Stokes shifts (120 nm) and the longest emission peak wavelength (720 nm). Photoinduced intramolecular electron transfer (PET) from TAC to the rhodamine analog quenched the fluorescence. In contrast, the fluorescence is recovered upon the addition of K^+ as PET will be inhibited during complexation between TAC and K^+. However, these small molecule-based sensors are significantly taken up by many cell types, and thus, their application in extracellular K^+ sensing is limited [6]. PET approach can be complex and difficult to optimise [12]. Also, these sensors were not reported for either intracellular or extracellular investigations. An ideal intracellular K^+ sensor should display wide dynamic K^+ detection range (100–300 mM), insensitive to Na^+ (5–15 mM in intracellular fluid) and other metal ions at physiological concentrations, insensitive to pH and give rapid response [1].

Na^+-specific DNAzyme [13,14], fluorescent organic nanoparticles from a Biginelli-based receptor [4], *etc.*, have been used in measuring Na^+ concentration in the physiological range. Supramolecular receptors based on crown ethers or cryptands have been developed with varying structural modifications to render them strong contenders, for sensing Na^+ in biomedical applications. Nevertheless, the efficiency of Na^+ sensor in aqueous media, complicated procedures, requisite for expensive setup and instrumentations are some of the shortcomings of the developed sensors. Also, the formation of highly stable complexes from crown ethers with sodium/potassium salts limits the usage and sensitivity of the sensors. This is because the high complex stability constants limit the reversibility of the complexation of the sensor and restrict the long term usage of the sensor [15].

Ribonucleases (RNases) play an important role in immune response regulation during infection and cancer [16]. Particularly, RNase A is the first and best-characterised enzyme in the RNase family since the early 20th century. RNase A is an endonuclease that catalyses the depolymerisation of RNA. RNase A recognises and cleaves the negatively charged phosphate groups (pyrimidine bases) at the 3′-end of the phosphodiester bond for binding with the purine bases at the 5′-end position [17]. Kong et al. reported the use of RNase A as a biological template in synthesising CdTe quantum dots [18], AuNCs [19] and PbS quantum dots [20], in 2010, 2013 and 2016, respectively. These RNase A-assisted synthesised nanomaterials have shown potential in targeted drug delivery, cancer imaging and therapy after functionalisation with targeting and imaging agents such as cyclic RGD peptides [18] and vitamin B_{12} [19].

Graphene is a promising nanomaterial for biosensing applications owing to its atomically thin nature, good bio-molecular compatibility and exceptional electrical properties [3]. It has been demonstrated that graphene-based devices can detect K^+ concentrations as low as 1 nM or even 2 pM [5]. Folic acid (FA) is a water-soluble B vitamin widely used in drug targeting due to its low cost, compatibility in organic and aqueous solvents and lack of immunogenicity [21]. Folate receptor (FR) is highly expressed (more than 90%) on primary and metastatic human cancer cells [22]. FAs have shown a high affinity for the FRs on cancer cells. Hence, FAs are commonly used as colon cancer biomarkers for precise targeting of pathologic cells, specifically without affecting the normal cells [23,24]. The covalent binding of FA to reduced graphene oxide (rGO) produces stable and biocompatible materials with potential as a biosensor or drug delivery carrier.

Monovalent cations such as Na^+ and K^+ bind to protein surfaces due to the local cation-specific interactions with the anionic carboxylate group in Glu and Asp side chains on the protein backbone [25]. Inspired by the interesting fact that RNase A can be activated by potassium and sodium salts, our group has designed an effective "turn-off/turn-on" fluorescent sensor to detect these two ions using RNase A/AuNCs. RNase A/AuNCs are firstly loaded onto FA-rGO for a fluorescence "turn-off", followed by the fluorescence "turn-on" after the addition of Na^+ and K^+.

Depending on the reaction conditions, protein-templated AuNCs are formed either under protein-denatured or native condition [26]. The encapsulation of AuNCs inside the protein template might interfere with the protein structure and activity. Since RNase A is a therapeutic protein, it is important to preserve the native protein structure to retain its biological activity after the formation of AuNCs. Although advanced analytical methods are available to investigate the protein activity, most depend on expert operators and capital equipment that are often low throughput and prohibitively expensive [27]. To the best of our knowledge, this is the first work done on studying the activity of protein RNase A in RNase A/AuNCs and exploring the potential application of RNase A/AuNCs towards sensing metal ions. Although the work is preliminary, the current design combines the potential of drug delivery, active targeting, and therapy of cancer cells and biosensing of metal ions in a single platform.

In brief, a novel metal ion sensor for the determination of Na^+ and K^+ based on "turn-off/turn-on" fluorescence has been constructed. The sensor possesses the following advantages: (1) composed of entirely biocompatible materials such as RNase A/AuNCs, FA and rGO (2) its excitation (365 nm) and emission (627 nm) wavelengths can minimise the effects of background fluorescence of biological fluids (3) the sensing model can be readily extended to the sensing of other cations by simply using other specific proteins on metal nanoclusters and even to the sensing of other biomolecules. This can be accomplished by the rational design employed, in which different interactions bring metal ions and functional groups on protein to close proximity. Hence, this investigation provides a new type of green nanomaterials for metal ions biosensing with potential in drug delivery [28], active targeting and therapy on cancer cells and biosensing of metal ions.

2. Experimental

2.1. Reagents and materials

Ribonuclease A from bovine pancreas (≥60%, Sigma) was purchased in lyophilised-powder form and used without further purification. Gold (III) chloride solution ($HAuCl_4$), folic acid (>97%), *N*-hydroxysuccinimide (NHS), *N*-(3-Dimethylaminopropyl)-*N*′-ethylcarbodiimide hydrochloride (EDC), ribonuclease A detection kit, and all other reagents were purchased from Sigma Aldrich and used as received. Ultrapure deionised water was obtained from a Milli-Q Plus system (EMD Millipore, Billerica, MA, USA). Sodium hydroxide (1 M, NaOH) was purchased from Nacalai Tesque. Potassium chloride (KCl) was purchased from Systerm. Sodium chloride (NaCl) and tris-hydrochloride (Tris-HCl) were purchased from Merck.

2.2. Analytical measurements

Fluorescence spectra were recorded using a fluorescence spectrophotometer (Hitachi F-7000). UV—vis absorbance was measured using a UV—vis spectrophotometer (Lambda 35, PerkinElmer) to ensure the absence of large nanoparticles (NPs), which commonly show a maximum absorption peak at about 520 nm. UV light with the excitation of 365 nm was used. To study the protein conformation, far-UV circular dichroism (CD, J-1000 series, JASCO) was employed. The oxidation state of core Au atoms was examined by X-ray photoelectron spectroscopy (XPS, ULVAC-PHI, Inc.). The morphological characterisation of RNase A/AuNCs was carried out using a high-resolution transmission electron microscope (HRTEM, FEI Tecnai G2 F20 X-Twin). The Fourier transform infrared spectroscopy (FTIR) spectra of FA, rGO and FA-rGO were recorded on an FTIR spectrometer (PerkinElmer Frontier).

2.3. Synthesis of RNase A/AuNCs

RNase A/AuNCs was synthesised following a protocol reported by our group [29]. Briefly, 0.7 mL of 12 mM $HAuCl_4$ solution was added to the same amount of aqueous solution containing 20 mg mL^{-1} RNase A in a thermomixer and mixed at 1200 rpm for 5 min at 40 °C. Then, 0.1 mL of 1 M NaOH solution was introduced, and the mixture was subjected to a thermomixer at 900 rpm for 6 h at 60 °C. The color change of the solution from light yellow to deep brown indicates the successful synthesis of RNase A/AuNCs. The resulting solution was purified using EMD Millipore Amicon Ultra-0.5 centrifugal filter unit with a membrane having a molecular weight cut-off (MWCO) of 10 kDa to remove residual ions (*i.e.* Na^+, Au^{3+} and OH^-). The products were then stored at 4 °C until further use.

2.4. RNase A protein activity assay

The detection of RNase A activity was performed by referring to the technical bulletin of the ribonuclease A detection kit. The assay was performed using microplates with a reaction volume of 200 μL. Briefly, control was prepared by mixing 100 μL of RNA solution and 100 μL of water. The blank was prepared by mixing 100 μL of reaction buffer and an equal amount of water. The absorbance of the control and blank were read by UV—vis spectroscopy at A_{300nm} of the control *vs* blank. The absorbance must be 0.73 ± 0.03 before beginning the assay. Total hydrolysis (E_f) was determined by preparing a triplicate of the mixture of 100 μL of RNA solution and 100 μL of 6 μg mL^{-1} RNase A. The spectrophotometer was calibrated against the blank. The absorbance of the triplicate was read at 25 °C for about 120 min at 1-min intervals or until the $\Delta A_{300\ nm}$/min is ˂0.002. To measure the rate determination (E_0), the spectrophotometer was calibrated against the blank. A mixture of 100 μL of RNA solution and 92 μL of water was prepared and equilibrated to 25 °C until A_{300nm} remained constant. 8 μL of 2.4 μg mL^{-1} RNase A was added to the mixture and immediately mixed by inversion. The decrease in A_{300nm} was recorded for about 10 min. The slope of the line ($\Delta A_{300\ nm}$/min) was then determined. Rate determination was repeated with 2.4 μg mL^{-1} RNase A/AuNCs samples (E_s). The slope of the line was determined using the following standard Eq. (1).

$$Slope = \Delta \ln\left(E_0 - E_f\right) \Big/ \Delta t \tag{1}$$

Kunitz units/mL enzyme was calculated using the following Eq. (2).

$$[(slope)(df)(V_F)] \,/\, (V_E) \tag{2}$$

where d_f is the dilution factor, V_F is the total volume of the assay (in millilitres), and V_E is the volume (in millilitres) of the enzyme used.

2.5. Preparation of reduced graphene oxide

Graphene oxide (GO), Ganoderma lucidum (GL) extract and rGO were synthesised following the protocol reported by our group [30]. Briefly, GO solution (0.1 mg mL^{-1}) was adjusted to pH 7 using NaOH. GL extract (50 mL) was added to a 50 mL of GO solution and transferred to a water bath preheated to 85 °C. The solution was mixed at 120 rpm for 16 h. The resulting solution was ultracentrifuged at 10,000 rpm for 20 min and washed three times with water before re-dispersing into water.

2.6. Covalent conjugation of FA-rGO

FA-rGO was prepared using a modified protocol reported by Zhang et al. (2010) [31]. Briefly, 1 mg mL^{-1} rGO was subjected to probe sonication (20 kHz, 500 W) for 10 min. NaOH (6.25 mmol) and chloroacetic acid (0.250 g, 11.655 mmol) were then added. The mixture was bath sonicated (40 kHz, 70 W) for 2 h. After neutralisation with HCl, the mixture was purified by repeated rinsing and centrifugation until rGO is well dispersed in deionised water. The mixture was dialysed against deionised water for 24 h. To introduce sulfonate groups to the rGO, aryl diazonium salt was prepared by dissolving sulfanilic acid (51.96 mg, 0.06 M) and sodium nitrite (70.720 mg, 0.205 M) in 20 mL of 0.25 v/v % 1 M NaOH. The solution was added dropwise to 0.1 M HCl in an ice bath. The diazonium salt solution was mixed with rGO in an ice bath under stirring for 2 h, followed by dialysis against deionised water for over 24 h. The mixture was stored at 4 °C until further use. EDC and NHS were added onto rGO, with the molar ratio of rGO:EDC:NHS as 40:50:73. The mixture was subjected to probe sonication for 2 h. FA

(5 mg mL^{-1}, dissolved in 0.5 M $NaHCO_3$, at pH 8) was added and stirred overnight. The products were dialysed against 0.5 M $NaHCO_3$ for 24 h, followed by dialysis against deionised water for over 24 h. The products were characterised by FTIR, UV−vis spectroscopy and fluorescence spectrophotometer.

2.7. Fluorescence quenching of RNase A/AuNCs by FA-rGO

To investigate the potential of FA-rGO to induce fluorescence quenching of RNase A/AuNCs, different concentrations of FA-rGO were added to 8 mg mL^{-1} of RNase A/AuNCs. The solution was mixed in a thermomixer at 900 rpm for 10 min at room temperature. The fluorescence intensity of the solution was recorded at an excitation wavelength (λ_{ex}) of 365 nm.

2.8. Sensing of potassium and sodium ions

The detection of K^+ and Na^+ ions were conducted as follows. The same volume of FA-rGO-RNase A/AuNCs was added with various concentrations of K^+. The solution was mixed in a thermomixer at 900 rpm for 20 min at room temperature. The fluorescence intensity was measured to quantify the concentration of K^+ at $\lambda_{ex} = 365$ nm. The steps were repeated for the detection of Na^+. The experiments were repeated with RNase A/AuNCs only, without FA-rGO.

2.9. Calculation of the signal-to-noise ratio and limit of detection

The signal-to-noise ratio (SNR) was calculated using the following Eq. (3).

$$SNR = R_L / S_1 \quad (3)$$

Limit of detection (LOD) was calculated based on the following Eqs. (4) and (5).

$$y = a + SX \quad (4)$$

where X is LOD.

$$y = (K \times S_1) + Blank \quad (5)$$

where,

$$a + (S \times LOD) = (K \times S_1) + Blank$$

Therefore,

$$LOD = [(K \times S_1) + Blank - a]/S$$

where R_L is the signal response of least known concentration, K is the coefficient, 3.3 [32], S is the slope obtained from the calibration curve, while S_1 is the statistical result of the standard deviation of the blank solution, and "a" is the blank value.

3. Results and discussion

3.1. Synthesis and characterisation of RNase A/AuNCs

HRTEM image (Fig. 1A) demonstrates the spherical-shaped RNase A/AuNCs, with cluster sizes within a narrow range of less than 2 nm, which agrees with protein-templated AuNCs reported previously [33]. As shown in the optical absorption of the as-prepared RNase A/AuNCs (Fig. 1B), no apparent surface plasmon resonance absorption peak could be observed in the range between 400 and 600 nm. The absence of the plasmon absorption at about 520 nm indicates the absence of any continuous density of states in RNase A/AuNCs [34]. The ultra-small size of AuNCs can no longer support the localised surface plasmon resonance effect, which typically contributes to the optical and electronic properties of gold NPs [19,35]. This confirms the encapsulation of AuNCs in RNase A protein, and most importantly, no large NPs (>2 nm in diameter) were formed [29,36].

Besides, the as-synthesised RNase A/AuNCs exhibited bright red fluorescence under UV irradiation (Fig. 1B), with the emission band at 645 nm when excited at 365 nm. The fluorescence of the RNase A/AuNCs was contributed by the ultraviolet-excitable amino acid residues such as tyrosine, histidine and phenylalanine in the RNase A protein [37]. Most of the fluorophores used for metal ions sensing have emission wavelength below 600 nm, leading to light-induced toxicity, weak tissue penetration and resolution, auto-fluorescence and light absorption of biomolecules [1]. The design of low-energy NIR fluorescent sensors with long-wavelength fluorescence is capable of overcoming the shortcomings mentioned above. The photoluminescence quantum yield (QYs) of RNase A/AuNCs was about 7.46% when calibrated with rhodamine B, which has a QYs of 31% in water when excited at 514 nm.

RNase A is a single domain protein with two-subdomain portions containing 124 amino acid residues comprising 3 α-helices, 7 short β-strands and loops connecting them. As shown in Fig. 2, the native RNase A is stabilised by four disulfide bonds (Cys26-Cys84, Cys40-Cys95, Cys58-Cys110 and Cys65-Cys72) and two *cis*-peptide bonds before prolines (Pro93 and Pro114). At a temperature higher than 50 °C, the protein becomes unstable as the high kinetic energy of the chain disrupts the protein structure. The protein is in a reversible transition state between unfolded and compact. However, the RNase A becomes completely denatured, compact and biologically inactive above 67 °C [38,39]. Therefore, a temperature of 60 °C was chosen for the synthesis instead of the physiological temperature (37 °C). This is because, upon heating, the Phe46 residues located in the hydrophobic core of RNase A will be replaced with other hydrophobic amino acid residues. This will result in a marked decrease in RNase A's thermal stability and unfolding of RNase A, making the compact native form of RNase A flexible and reactive [40]. A higher interaction between RNase A and Au ions fastens the formation of RNase A/AuNCs.

XPS was employed to investigate the protein-AuNCs interactions and prove the protein's reducibility against Au(III) ions in alkaline pH (Fig. S1 in the supplementary data). As shown in Fig. S1A in the supplementary data, the XPS of Au 4f and the binding energies at 83.811 eV (Au $4f_{7/2}$) and 87.311 eV (Au $4f_{5/2}$) confirm the formation of stable RNase A/AuNCs, with most of the Au atoms close to the oxidation state of Au(0) [19]. The two S 2p bands with the binding energies of about 163 (S $2p_{1/2}$) and 169 eV (S $2p_{3/2}$) were observed (Fig. S1B in the supplementary data), corresponding to the gold-bound (Au-S) and oxidised sulfur species, respectively.

CD spectroscopy was employed further to investigate the conformational evolution of native and AuNCs-bound proteins. From the CD spectra, as shown in Fig. S2 in the supplementary data, a broad negative band with protrusions at 209 nm for α-helix and 218 nm for β-sheet was observed for RNase A. Attributed to the nucleation of AuNCs, the intensity of α-helix peaks declines with the addition of Au. It shows a 100% reduction in the α-helix and a 31% decrease in the β-sheet after the synthesis of RNase A/AuNCs. The valley at 218 nm becomes markedly shallower. Blue shifts to about 198 nm after the cluster formation, indicating an increase in the disordered and random coil structures in the RNase A/AuNCs (due to protein unfolding). Therefore, it can be deduced that the interaction between these molecules are complex and cause multidirectional alterations in the protein structure.

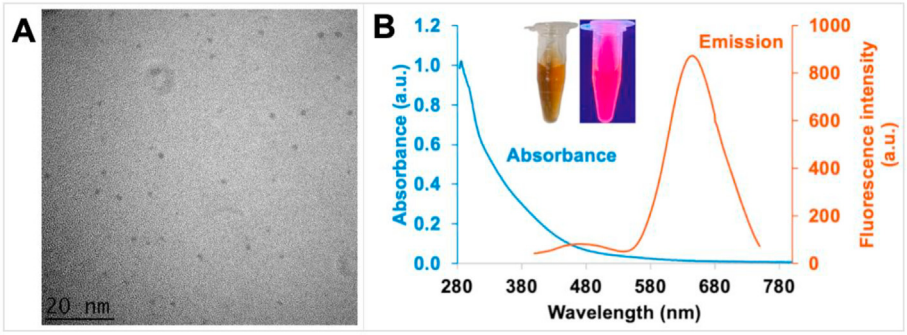

Fig. 1. Characterisation of RNase A/AuNCs (A) HRTEM image of the diluted fluorescent RNase A/AuNCs (B) UV–vis absorption (blue line) and fluorescence emission spectra (orange line) of the as-prepared RNase A/AuNCs with λ_{ex} at 365 nm. Inset: Optical photographs of the RNase A/AuNCs under visible (left) and UV light (right). (For interpretation of the references to color in this figure legend, the reader is referred to the Web version of this article.)

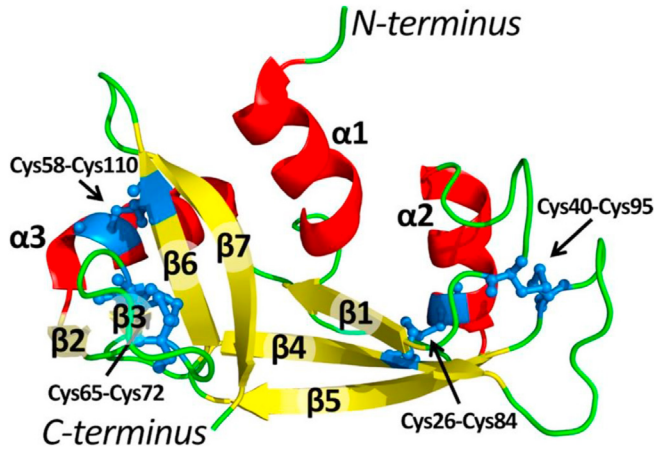

Fig. 2. Characterisation of RNase A/AuNCs. Cartoon representation of RNase A (Reprinted with permission from Ref. [33], ACS Publications, 2017).

3.2. RNase A protein activity assay

UV spectroscopy is a fast, simple and inexpensive method to determine the protein activity or structure, as well as protein-protein and protein-ligand interactions [27]. RNase A converts RNA to oligonucleotides in the presence of water. RNase A primarily absorbs UV light with absorbance maxima at 300 nm. Hence, RNase A activity was calculated after monitoring the decrease in absorbance at 300 nm upon hydrolysis at 25 °C. Total hydrolysis (E_f) was determined by plotting a graph of absorbance *vs* time (Fig. S3A in the supplementary data). The slope of the line was observed as 0.6417. Rate determination of RNase and RNase/AuNCs *vs* blank were plotted (Fig. S3B in the supplementary data). The graphs of $\ln(E_0\text{-}E_f)$ and $\ln(E_s\text{-}E_f)$ *vs* time were plotted (Fig. S3C in the supplementary data). The final activity of RNase A samples was calculated using Eq. (2). The RNase A in the RNase A/AuNCs sample was 50.8% active and can exert ribonucleolytic activity against RNA [41,42].

3.3. Loading of RNase A/AuNCs onto FA-rGO

Functionalisation of biomolecules on the surface of GO-based nanosystem enhances the catalytic activity, leading to an increase in the electrode surface area and active sites for electron capture in solution. The GO-based nanosystem owns π-π stacking interaction, which induces facile electron transfer between the nanosystem and target analytes [43,44]. FA-rGO targets the folate receptor-positive cancer cells and acts as a novel nanocarrier for the co-delivery of genes and drugs for enhanced cancer therapy [45]. The loading of RNase A/AuNCs onto FA-rGO was driven by hydrophobic interactions and π-π stacking between RNase A/AuNCs and aromatic regions of the rGO sheets [46]. Graphene-based oxides are known to decrease the photo-emission of the fluorescent molecule *via* the photoinduced charge transfer from the fluorophore to the oxide surface [47]. The interaction of RNase A/AuNCs with either the metallic core, the stabiliser or the linkage between these two might interfere with the fluorescence properties [48]. The charge transfer from RNase A/AuNCs to FA-rGO weakens the Au-S bond between cysteine residues and the Au core, which in turn reduces charge transfer from RNase A ligands to AuNCs, leading to the fluorescence quenching of AuNCs [35,44,49,50]. As displayed in Fig. 3, the higher the concentrations of FA-rGO, the higher the fluorescence quenching of RNase A/AuNCs. A relative concentration of 50 μg mL^{-1} of FA-rGO was chosen since the fluorescence of RNase A/AuNCs was quenched by about 15%.

3.4. Effect of addition of potassium and sodium ions on the fluorescence intensity of RNase A/AuNCs and FA-rGO-RNase A/AuNCs

K^+ is one of the predominant ions in living cells with an extracellular concentration (in serum) of around 3.5–5.3 mM [1,6,7]. The normal concentrations of K^+ are about 40–120 mM in urine, 5–10 mM in sweat and about 30 mM in saliva [51]. Erythrocytes and epidermal cells have higher intracellular K^+ with homeostasis concentrations of 200 and 475 mM, respectively, while the intracellular K^+ concentration for myocytes is even higher (at mole levels) [11].

Despite the excellent sensitivity and selectivity, most of the current nanomaterial-based Na^+ and K^+ biosensors (Table 1) present several drawbacks for wider biological applications, such as lengthy experimental procedures, requisite for expensive instrumental setups, results are easily affected by photobleaching and light scattering, materials with limited toxicity studies, *etc*. For example, commercially available K^+ biosensor, such as potassium-binding benzofuranisophthalate (PBFI), has a relatively large dissociation constant (K_d) (up to 6.6 mM) [52], which is not ideal for highly concentrated intracellular K^+ sensing. Therefore, it is desirable to fabricate Na^+ and K^+ biosensors that can be constructed in a facile protocol, cost-effective, biocompatible, capable of measuring quickly, with a fluorescence emission wavelength of over 600 nm, and without any reference solution.

In this study, the effect of the addition of Na^+ and K^+ ions on the fluorescence intensity of RNase A/AuNCs and FA-rGO-RNase A/

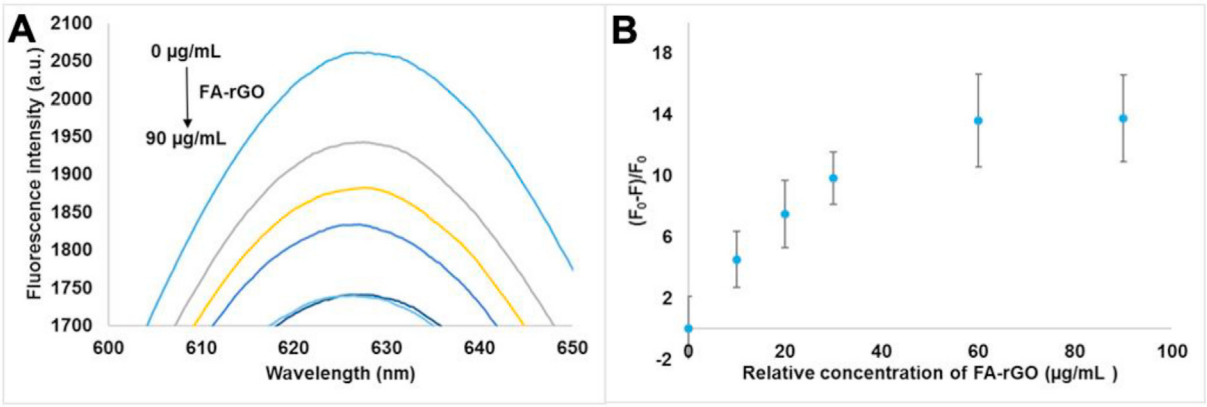

Fig. 3. Effect of addition of FA-rGO onto RNase A/AuNCs (A) Fluorescence intensity of 8 mg mL^{-1} of RNase A/AuNCs at λ_{ex} = 365 nm, by varying the concentration of FA-rGO. The relative concentrations of FA-rGO were 0, 10, 20, 30, 60 and 90 µg mL^{-1} (B) Fluorescence quenching values of 8 mg mL^{-1} of RNase A/AuNCs by varying the concentration of FA-rGO. Inset: Error bars indicate the standard deviation of three independent measurements.

Table 1
Examples of K^+ and Na^+ biosensors with their sensitivity and linear range values as reported in the literature.

Type of metal ion biosensor	Schematic biosensor assembly	Signal	Linear range	Limit of detection	Reference
Potassium ion	CVD-grown single-layer graphene	Electrical	1 nM-10 µM	1 nM	[3]
	Gold nanoparticles and a dye (Cationic Yellow 5 GL)	Colorimetric	10 nM-50 mM	4.4 nM	[51]
	Berberine–G-quadruplex complex	Fluorescence	0.005 –1.0 mM	2 µM	[7]
	Triazacryptand with a rhodamine analog		16–400 mM	–	[1]
	Dye OliGreen (OG) and ATP-binding aptamer		100 –1000 nM	75 nM	[2]
	Aminated carbon dots and 18C6E-reduced graphene oxide hybrids		0.05 –10.0 mM	10 µM	[55]
	2-dicyanomethylene-3-cyano-4,5,5-trimethyl-2,5-dihydrofuran (TCF) and triazacryptand (TAC)		0–1600 mM	–	[11]
	Triazacryptand with polymers (HEMA, AM, METAC, MESA)		0–200 mM	–	[6]
	RNase A/AuNCs		0–200 mM	74 mM	Present work
	FA-rGO-RNase A/AuNCs		0–25 mM	15.7 mM	Present work
	Solution-gated CVD graphene with hydrophilisation pretreatment	Electrochemical	0.1 pM-100 nM	0.058 pM	[5]
	Ordered mesoporous carbon (OMC) sphere		$10^{-4.19}$-$10^{-0.21}$ M	5.4 µM	[56]
	Manganese oxide nanorods		2–90 µM	0.05 µM	[57]
	4-aminobenzo-18-crown-6 on a functionalised gold surface		0.1–7 mM	–	[10]
	Valinomycin doped chitosan-graphene oxide thin film	Surface plasmon resonance	0–100 ppm	0.001 ppm/ 0.02557 µM	[9]
	Silver nanoplasmon	Surface-enhanced Raman scattering	50–3000 nM	25 nM	[58]
Sodium ion	G-quadruplex formed by p25	Colorimetric	20 µM-0.8 mM	0.6 µM	[14]
	Covalently linked aminorhodamine B-calix [4]arene chromoionophore	Fluorescence	0.01–2.0 M	–	[12]
	Organic nanoparticles (Biginelli compound 1)		0–40 µM	22 nM	[4]
	RNase A/AuNCs		0–100 mM	49 mM	Present work
	FA-rGO-RNase A/AuNCs		0–200 mM	110 mM	Present work
	Silver nanoparticles/graphene oxide nanocomposite	Electrochemical	0–100 mM	9.344 mM	[43]

AuNCs is investigated. As depicted in Figs. S4A–S4C in the supplementary data, the addition of K^+ into RNase A/AuNCs increased its fluorescence, with a linear dynamic range from 0 to 800 mM and a LOD of 74 mM. On the other hand, Fig. 4A–C shows that the addition of K^+ into FA-rGO-RNase A/AuNCs recovered its fluorescence, with a linear dynamic range from 0 to 125 mM and a LOD of 15.7 mM under physiological conditions (pH 7.4). It is observed that the nanoplatform, which firstly quenched with FA-rGO, can achieve 4.7-fold lower LOD than the nanoplatform with RNase A/AuNCs only. Both these nanoplatforms exhibit "turn-on" fluorescence of about 14–15% and are sufficiently sensitive to detect the intracellular concentrations of K^+, which is typically about 150 mM.

Clinical trials showed that the recommended Na^+ intake in adults should be below 100 mmol (about 2.3 g of Na^+ or 5.8 g of salt per day) [43]. Any deviation in the blood ionic equilibrium may increase the risk of stroke, heart failure, diabetes and kidney problems [4,14,43]. As shown in Figs. S5A–S5C in the supplementary data, the addition of Na^+ into the RNase A/AuNCs enhanced its

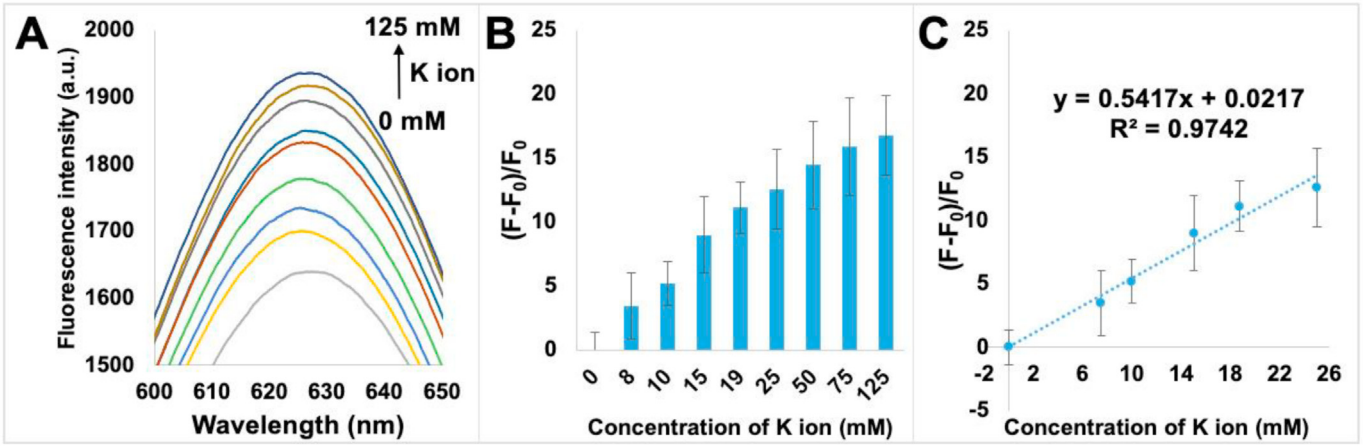

Fig. 4. Sensitive detection of potassium ion using FA-rGO-RNase A/AuNCs (A) Fluorescence intensity of FA-rGO-RNase A/AuNCs by varying the concentration of potassium ion. The relative concentrations of potassium ion were 0, 7.5, 10, 15, 8.75, 25, 50, 75 and 125 mM at λ_{ex} = 365 nm (B) Relationship between the fluorescence recovery values $(F\text{-}F_0)/F_0$ and the target concentrations (C) Linear response of the fluorescence recovery values $(F\text{-}F_0)/F_0$ to the concentration of potassium ion. Error bars are the standard deviation of three repetitive experiments.

fluorescence, with a linear dynamic range from 0 to 700 mM and a LOD of 49 mM. Meanwhile, Fig. 5A–C demonstrates that the addition of Na^+ into FA-rGO-RNase A/AuNCs recovered its fluorescence, with a linear dynamic range from 0 to 1000 mM and a LOD of 110 mM of Na^+ under a pH of 7.4. There is a saturation effect observed over 200 mM of Na^+. The nanoplatform with RNase A/AuNCs achieved only 2.2-fold lower LOD than the nanoplatform that firstly quenched with FA-rGO. Both these nanoplatforms displayed a "turn-on" fluorescence of about 19–20% and are satisfactory to detect the normal concentration of Na^+ in serum which is around 135–148 mM under physiological conditions [4,7].

It is speculated that the fluorescence "turn-on" mechanism after the addition of Na^+ and K^+ is due to PET. PET is a method for the sensitive detection of cations in solution based on a host-guest (ion) recognition site that is covalently linked to a chromophore [12]. Na^+ and K^+ binding to the protein RNase A surface is due to the local cation-specific interactions with the anionic carboxylate group in Glu and Asp side chains on the protein backbone [25].

Na^+ and K^+ possess the same charge and are closely similar in ionic radius (116 and 152 p.m., respectively) and spatial orbital design [51]. Even though Na^+ has a smaller ionic radius, but it possesses a higher charge density and larger hydrated radius than K^+ [53]. Based on the simple electrostatic arguments, a cation and an anion with similar hydration energies tend to form contact ion pairs in aqueous solutions. Na^+ tends to bind stronger and has a higher affinity (at least twice) to the anionic groups on the protein surface than K^+ [25]. For example, RNase A protein effectively binds to 1–2 Na^+ and fewer than half the number of K^+ [25]. At the same time, Na^+ becomes more strongly hydrated than K^+ as the free energy barrier increases. The removal of one water molecule from the first hydration shell (to facilitate a direct contact) becomes increasingly difficult [54]. Eventually, the ion binding kinetics of Na^+ gets slower. Therefore, it can be observed that the fluorescence recovery of RNase A/AuNCs after the addition of Na^+ was higher with higher LOD than K^+.

Another possible mechanism of the fluorescence "turn-on" after the addition of Na^+ and K^+ could be due to the oxidation/reduction reactions. In an aqueous solution, water molecules dissociate to form hydrogen and hydroxyl ions that can be adsorbed onto most metal oxide. The metal ions diffuse into RNase A/AuNCs and

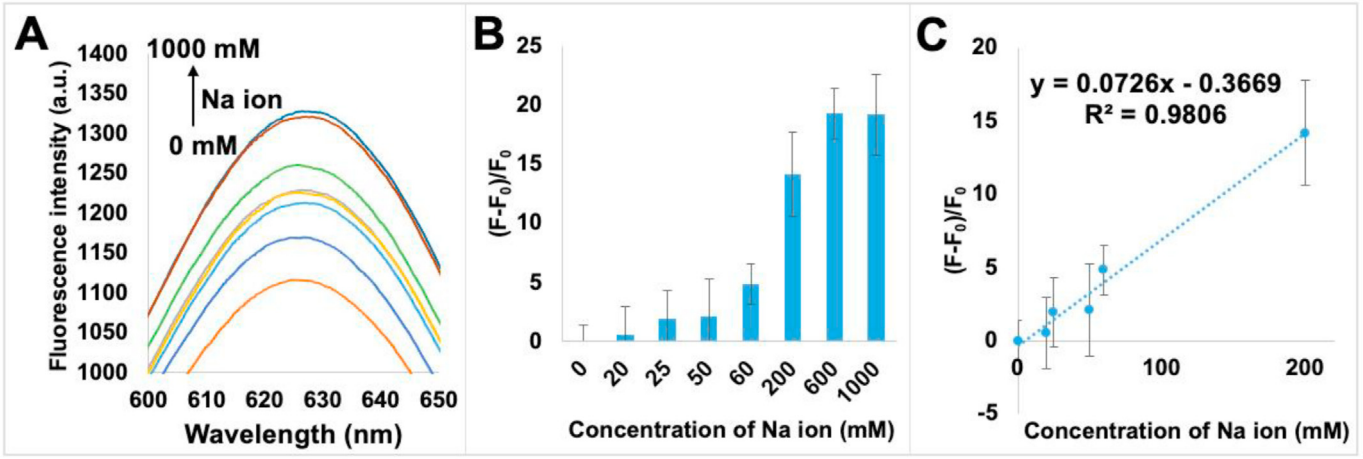

Fig. 5. Sensitive detection of sodium ion using FA-rGO-RNase A/AuNCs (A) Fluorescence intensity of FA-rGO-RNase A/AuNCs by varying the concentration of sodium ion. The relative concentrations of sodium ion were 0, 20, 25, 50, 60, 200, 600 and 1000 mM at λ_{ex} = 365 nm (B) Relationship between the fluorescence recovery values $(F\text{-}F_0)/F_0$ and the target concentrations (C) Linear response of the fluorescence recovery values $(F\text{-}F_0)/F_0$ to the concentration of sodium ion. Error bars are the standard deviation of three repetitive experiments.

interact *via* ion-exchange reactions with positive and negative sweeps on the protein and FA-rGO surfaces. They donate/accept a proton from the solution to form a negative and positive surface group, respectively [43]. Therefore, the fluorescence intensity of RNase A/AuNCs is recovered upon binding to Na^+ and K^+.

4. Conclusions

In this study, a novel nanobiosensor for detecting metal ions using RNase A/AuNCs-based platform has been reported. RNase A/AuNCs is synthesised using a facile and optimised protocol. The activity of RNase A protein after the formation of RNase A/AuNCs is investigated using RNA detection, in which 50.8% of RNase A was found to be active in RNase A/AuNCs. RNase A/AuNCs then loaded onto FA-rGO. FA-rGO is used as a potential carrier and fluorescence quencher for RNase A/AuNCs. Finally, a fluorescence turn-on sensing strategy is developed using the as-synthesised FA-rGO-RNase A/AuNCs to detect Na^+ and K^+ ions. The developed nanobiosensor reveals an excellent sensing performance and meets the sensitivity required to detect both intracellular Na^+ and K^+ ions. Although the selectivity data for the nanobiosensor have not been investigated, the selectivity is expected to increase following pre-treatment with blocking agents such as *N*-ethylmaleimide. To the best of our knowledge, this is the first work done on exploring the potential application of RNase A/AuNCs as a metal ion sensor. This work serves as a proof-of-concept for combining the potential of drug delivery, active targeting and therapy on cancer cells and biosensing of metal ions into a single platform.

CRediT authorship contribution statement

Xin Yi Wong: Conceptualization, Investigation, Methodology, Writing – original draft, Writing – review & editing. **Daniel Quesada-González:** Data curation, Formal analysis, Writing – review & editing. **Sivakumar Manickam:** Data curation, Formal analysis, Supervision, Writing – review & editing. **Kasturi Muthoosamy:** Data curation, Formal analysis, Funding acquisition, Supervision, Writing – review & editing.

Declaration of competing interest

The authors declare that they have no known competing financial interests or personal relationships that could have appeared to influence the work reported in this paper.

Acknowledgements

This work was supported by the Fundamental Research Grant Scheme (FRGS), Ministry of Higher Education (MOHE), Malaysia (FRGS/1/2016/STG07/UNIM/02/1), the Royal Society-Newton Mobility Grant with Newton-Ungku Omar Fund, Academy of Sciences Malaysia (NMG\R1\180496).

Appendix A. Supplementary data

Supplementary data to this article can be found online at https://doi.org/10.1016/j.aca.2021.338745.

References

[1] G. Song, D. Jiang, L. Wang, J. Ning, X. Sun, F. Su, M. Chen, Y. Tian, A mitochondria-targeting NIR fluorescent potassium ion sensor: real-time investigation of the mitochondrial K^+ regulation of apoptosis *in situ*, Chem. Commun. 56 (2020) 5405–5408.
[2] C.C. Huang, H.T. Chang, Aptamer-based fluorescence sensor for rapid detection of potassium ions in urine, Chem. Commun. 12 (2008) 1461–1463.
[3] X. Liu, C. Ye, X. Li, N. Cui, T. Wu, S. Du, Q. Wei, L. Fu, J. Yin, C. Te Lin, Highly sensitive and selective potassium ion detection based on graphene hall effect biosensors, Materials 11 (2018) 399.
[4] G. Kaur, N. Kaur, Estimation of sodium ions using easily engineered organic nanoparticles-based turn-on fluorescent sensor: application in biological and environmental samples, Sensor. Actuator. B Chem. 265 (2018) 134–141.
[5] Q. Yuan, S. Wu, C. Ye, X. Liu, J. Gao, N. Cui, P. Guo, G. Lai, Q. Wei, M. Yang, W. Su, H. Li, N. Jiang, L. Fu, D. Dai, C.-T. Lin, K.W.A. Chee, Sensitivity enhancement of potassium ion (K^+) detection based on graphene field-effect transistors with surface plasma pretreatment, Sensor. Actuator. B Chem. 285 (2019) 333–340.
[6] X. Zhou, F. Su, W. Gao, Y. Tian, C. Youngbull, R.H. Johnson, D.R. Meldrum, Triazacryptand-based fluorescent sensors for extracellular and intracellular K^+ sensing, Biomaterials 32 (2011) 8574–8583.
[7] Y. Liu, B. Li, D. Cheng, X. Duan, Simple and sensitive fluorescence sensor for detection of potassium ion in the presence of high concentration of sodium ion using berberine-G-quadruplex complex as sensing element, Microchem. J. 99 (2011) 503–507.
[8] I. Kim, J.-E. Jung, W. Lee, S. Park, H. Kim, Y.-D. Jho, H.Y. Woo, K. Kyhm, Two-step energy transfer dynamics in conjugated polymer and dye-labeled aptamer-based potassium ion detection assay, Polymers 11 (2019) 1206.
[9] A.A. Zainudin, Y.W. Fen, N.A. Yusof, S.H. Al-Rekabi, M.A. Mahdi, N.A.S. Omar, Incorporation of surface plasmon resonance with novel valinomycin doped chitosan-graphene oxide thin film for sensing potassium ion, Spectrochim. Acta Mol. Biomol. Spectrosc. 191 (2018) 111–115.
[10] S. Kumbhat, U. Singh, A potassium-selective electrochemical sensor based on crown-ether functionalized self assembled monolayer, J. Electroanal. Chem. 809 (2018) 31–35.
[11] X. Zhou, F. Su, Y. Tian, C. Youngbull, R.H. Johnson, D.R. Meldrum, A new highly selective fluorescent K^+ sensor, J. Am. Chem. Soc. 133 (2011) 18530–18533.
[12] J.S. Benco, H.A. Nienaber, W. Grant McGimpsey, A sodium ion sensor based on a covalently-linked aminorhodamine B–calix[4]arene chromoionophore, Sensor. Actuator. B Chem. 85 (2002) 126–130.
[13] E.H. Kim, E.-S. Lee, D.Y. Lee, Y.-P. Kim, Facile determination of sodium ion and osmolarity in artificial tears by sequential DNAzymes, Sensors 17 (2017) 2840.
[14] H. Sun, H. Chen, X. Zhang, Y. Liu, A. Guan, Q. Li, Q. Yang, Y. Shi, S. Xu, Y. Tang, Colorimetric detection of sodium ion in serum based on the G-quadruplex conformation related DNAzyme activity, Anal. Chim. Acta 912 (2016) 133–138.
[15] A. Giovannitti, C.B. Nielsen, J. Rivnay, M. Kirkus, D.J. Harkin, A.J.P. White, H. Sirringhaus, G.G. Malliaras, I. McCulloch, Sodium and potassium ion selective conjugated polymers for optical ion detection in solution and solid state, Adv. Funct. Mater. 26 (2016) 514–523.
[16] E. Boix, F. Acquati, D. Leonidas, D. Pulido, Role of ribonucleases in immune response regulation during infection and cancer, Front. Immunol. 11 (2020) 236.
[17] M.V. Nogués, M. Vilanova, C.M. Cuchillo, Bovine pancreatic ribonuclease A as a model of an enzyme with multiple substrate binding sites, Biochim. Biophys. Acta Protein Struct. Mol. Enzymol. 1253 (1995) 16–24.
[18] Y. Kong, J. Chen, F. Gao, W. Li, X. Xu, O. Pandoli, H. Yang, J. Ji, D. Cui, A multifunctional ribonuclease–A–conjugated CdTe quantum dot cluster nanosystem for synchronous cancer imaging and therapy, Small 6 (2010) 2367–2373.
[19] Y. Kong, J. Chen, F. Gao, R. Brydson, B. Johnson, G. Heath, Y. Zhang, L. Wu, D. Zhou, Near-infrared fluorescent ribonuclease-A-encapsulated gold nanoclusters: preparation, characterization, cancer targeting and imaging, Nanoscale 5 (2013) 1009–1017.
[20] Y. Kong, J. Chen, H. Fang, G. Heath, Y. Wo, W. Wang, Y. Li, Y. Guo, S.D. Evans, S. Chen, D. Zhou, Highly fluorescent ribonuclease-A-encapsulated lead sulfide quantum dots for ultrasensitive fluorescence *in vivo* imaging in the second near-infrared window, Chem. Mater. 28 (2016) 3041–3050.
[21] F. Likis, Folic acid, J. Midwifery Wom. Health 61 (2016) 673–674.
[22] J.J. Yin, S. Sharma, S.P. Shumyak, Z.X. Wang, Z.W. Zhou, Y. Zhang, P. Guo, C.Z. Li, J.R. Kanwar, T. Yang, S.S. Mohapatra, W. Liu, W. Duan, J.C. Wang, Q. Li, X. Zhang, J. Tan, L. Jia, J. Liang, M.Q. Wei, X. Li, S.F. Zhou, Synthesis and biological evaluation of novel folic acid receptor-targeted, β-cyclodextrin-based drug complexes for cancer treatment, PloS One 8 (2013), e62289.
[23] Y. Wang, C. Dai, X.-P. Yan, Fabrication of folate bioconjugated near-infrared fluorescent silver nanoclusters for targeted *in vitro* and *in vivo* bioimaging, Chem. Commun. 50 (2014), 14341.
[24] A.K. Sahoo, U. Goswami, D. Dutta, S. Banerjee, A. Chattopadhyay, S.S. Ghosh, Silver nanocluster embedded composite nanoparticles for targeted prodrug delivery in cancer theranostics, ACS Biomater. Sci. Eng. 2 (2016) 1395–1402.
[25] L. Vrbka, J. Vondrášek, B. Jagoda-Cwiklik, R. Vácha, P. Jungwirth, Quantification and rationalization of the higher affinity of sodium over potassium to protein surfaces, Proc. Natl. Acad. Sci. Unit. States Am. 103 (2006) 15440–15444.
[26] Y. Xu, J. Sherwood, Y. Qin, D. Crowley, M. Bonizzoni, Y. Bao, The role of protein characteristics in the formation and fluorescence of Au nanoclusters, Nanoscale 6 (2014) 1515–1524.
[27] A.B. Biter, J. Pollet, W.-H. Chen, U. Strych, P.J. Hotez, M.E. Bottazzi, A method to probe protein structure from UV absorbance spectra, Anal. Biochem. 587 (2019), 113450.
[28] X.Y. Wong, A. Sena-Torralba, R. Alvarez-Diduk, K. Muthoosamy, A. Merkoçi, Nanomaterials for nanotheranostics: tuning their properties according to disease needs, ACS Nano 14 (2020) 2585–2627.

[29] X.Y. Wong, D. Quesada-González, S. Manickam, S.Y. New, K. Muthoosamy, A. Merkoçi, Integrating gold nanoclusters, folic acid and reduced graphene oxide for nanosensing of glutathione based on "turn-off" fluorescence, Sci. Rep. 11 (2021) 2375.
[30] K. Muthoosamy, R. Geetha Bai, I.B. Abubakar, S.M. Sudheer, H.N. Lim, H.S. Loh, N.M. Huang, C.H. Chia, S. Manickam, Exceedingly biocompatible and thin-layered reduced graphene oxide nanosheets using an eco-friendly mushroom extract strategy, Int. J. Nanomed. 10 (2015) 1505–1519.
[31] L. Zhang, J. Xia, Q. Zhao, L. Liu, Z. Zhang, Functional graphene oxide as a nanocarrier for controlled loading and targeted delivery of mixed anticancer drugs, Small 6 (2010) 537–544.
[32] D.A. Armbruster, T. Pry, Limit of blank, limit of detection and limit of quantitation, Clin. Biochem. Rev. 29 (2008) S49–S52.
[33] Y. Tao, M. Li, J. Ren, X. Qu, Metal nanoclusters: novel probes for diagnostic and therapeutic applications, Chem. Soc. Rev. 44 (2015) 8636–8663.
[34] D.S. Yarramala, A. Baksi, T. Pradeep, C.P. Rao, Green synthesis of protein-protected fluorescent gold nanoclusters (AuNCs): reducing the size of AuNCs by partially occupying the Ca^{2+} site by La^{3+} in Apo-α-lactalbumin, ACS Sustain. Chem. Eng. 5 (2017) 6064–6069.
[35] J. Olesiak-Banska, M. Waszkielewicz, P. Obstarczyk, M. Samoc, Two-photon absorption and photoluminescence of colloidal gold nanoparticles and nanoclusters, Chem. Soc. Rev. 48 (2019) 4087–4117.
[36] H. Li, Y. Cheng, Y. Liu, B. Chen, Fabrication of folic acid-sensitive gold nanoclusters for turn-on fluorescent imaging of overexpression of folate receptor in tumor cells, Talanta 158 (2016) 118–124.
[37] Y. Guo, H.T.N.N. Amunyela, Y. Cheng, Y. Xie, H. Yu, W. Yao, H.-W. Li, H. Qian, Natural protein-templated fluorescent gold nanoclusters: syntheses and applications, Food Chem. 335 (2021) 127657.
[38] C.M. Phillips, Y. Mizutani, R.M. Hochstrasser, Ultrafast thermally induced unfolding of RNase A, Proc. Natl. Acad. Sci. Unit. States Am. 92 (1995) 7292–7296.
[39] H. Fabian, H.H. Mantsch, Ribonuclease A revisited: infrared spectroscopic evidence for lack of native-like secondary structures in the thermally denatured state, Biochemistry 34 (1995) 13651–13655.
[40] T. Kadonosono, E. Chatani, R. Hayashi, H. Moriyama, T. Ueki, Minimization of cavity size ensures protein stability and folding: structures of Phe46-replaced bovine pancreatic RNase A, Biochemistry 42 (2003) 10651–10658.
[41] G. Gotte, M. Menegazzi, Biological activities of secretory RNases: focus on their oligomerization to design antitumor drugs, Front. Immunol. 10 (2019) 2626.
[42] R. Shapiro, B.L. Vallee, Site-directed mutagenesis of histidine-13 and histidine-114 of human angiogenin. Alanine derivatives inhibit angiogenin-induced angiogenesis, Biochemistry 28 (1989) 7401–7408.
[43] P. Traiwatcharanon, W. Siriwatcharapiboon, C. Wongchoosuk, Electrochemical sodium ion sensor based on silver nanoparticles/graphene oxide nanocomposite for food application, Chemosensors 8 (2020) 58.
[44] X. Wen, P. Yu, Y.-R. Toh, Y.-C. Lee, K.-Y. Huang, S. Huang, S. Shrestha, G. Conibeer, J. Tang, Ultrafast electron transfer in the nanocomposite of the graphene oxide–Au nanocluster with graphene oxide as a donor, J. Mater. Chem. C 2 (2014) 3826–3834.
[45] Q. Sun, X. Wang, C. Cui, J. Li, Y. Wang, Doxorubicin and anti-VEGF siRNA co-delivery *via* nano-graphene oxide for enhanced cancer therapy *in vitro* and *in vivo*, Int. J. Nanomed. 13 (2018) 3713–3728.
[46] Y. Wang, J.-T. Chen, X.-P. Yan, Fabrication of transferrin functionalized gold nanoclusters/graphene oxide nanocomposite for turn-on near-infrared fluorescent bioimaging of cancer cells and small animals, Anal. Chem. 85 (2013) 2529–2535.
[47] M.K. Kumawat, M. Thakur, R. Bahadur, T. Kaku, P. RS, A. Ninawe, R. Srivastava, Preparation of graphene oxide-graphene quantum dots hybrid and its application in cancer theranostics, Mater. Sci. Eng. C 103 (2019), 109774.
[48] H. Meng, D. Yang, Y. Tu, J. Yan, Turn-on fluorescence detection of ascorbic acid with gold nanoclusters, Talanta 165 (2017) 346–350.
[49] Y. Lin, P. Charchar, A.J. Christofferson, M.R. Thomas, N. Todorova, M.M. Mazo, Q. Chen, J. Doutch, R. Richardson, I. Yarovsky, M.M. Stevens, Surface dynamics and ligand–core interactions of quantum sized photoluminescent gold nanoclusters, J. Am. Chem. Soc. 140 (2018) 18217–18226.
[50] H.-H. Deng, K.-Y. Huang, S.-B. He, L.-P. Xue, H.-P. Peng, D.-J. Zha, W.-M. Sun, X.-H. Xia, W. Chen, Rational design of high-performance donor–linker–acceptor hybrids using a schiff base for enabling photoinduced electron transfer, Anal. Chem. 92 (2020) 2019–2026.
[51] M. Naderi, M. Hosseini, M.R. Ganjali, Naked-eye detection of potassium ions in a novel gold nanoparticle aggregation-based aptasensor, Spectrochim. Acta Mol. Biomol. Spectrosc. 195 (2018) 75–83.
[52] G. Song, R. Sun, J. Du, M. Chen, Y. Tian, A highly selective, colorimetric, and environment-sensitive optical potassium ion sensor, Chem. Commun. 53 (2017) 5602–5605.
[53] G. Gao, Y. Cao, W. Liu, D. Li, W. Zhou, J. Liu, Fluorescent sensors for sodium ions, Anal. Methods 9 (2017) 5570–5579.
[54] S. Cruz-León, N. Schwierz, Hofmeister series for metal-cation–RNA interactions: the interplay of binding affinity and exchange kinetics, Langmuir 36 (2020) 5979–5989.
[55] W. Wei, C. Xu, J. Ren, B. Xu, X. Qu, Sensing metal ions with ion selectivity of a crown ether and fluorescence resonance energy transfer between carbon dots and graphene, Chem. Commun. 48 (2012) 1284–1286.
[56] Z. Jiang, X. Xi, S. Qiu, D. Wu, W. Tang, X. Guo, Y. Su, R. Liu, Ordered mesoporous carbon sphere-based solid-contact ion-selective electrodes, J. Mater. Sci. 54 (2019) 13674–13684.
[57] M.-S. Ahn, R. Ahmad, J.-Y. Yoo, Y.-B. Hahn, Synthesis of manganese oxide nanorods and its application for potassium ion sensing in water, J. Colloid Interface Sci. 516 (2018) 364–370.
[58] C. Li, Y. Peng, H. Wang, A. Liang, Z. Jiang, A nanosol SERS method for quantitative analysis of trace potassium based on aptamer recognition and silver nanorod catalysis of Ag(I)-glucose reaction, Sensor. Actuator. B Chem. 281 (2019) 53–59.